2014 American Control Conference (ACC)
June 4-6, 2014. Portland, Oregon, USA

Preliminary Results on Identification of an Electro-Thermal Model for Low Temperature and High Power Operation of Cylindrical Double Layer Ultracapacitors

Yasha Parvini[1] Jason B. Siegel[2] Anna G. Stefanopoulou[2] Ardalan Vahidi[1]

Abstract— **The capability of ultracapacitors in delivering high power at low temperature applications such as cold starting is the motivation of this paper. A two state equivalent electric circuit model coupled with a two state thermal model is defined and parameterized to develop a four state control oriented electro-thermal model for cylindrical double layer ultracapacitors. The proposed two state equivalent electric circuit model mimics the terminal voltage dynamics and could be used to evaluate the power capability and efficiency of the cell. The electric model parameters are estimated by pulse-relaxation tests for sub-zero temperatures as low as -40 °C. The two state thermal model provides a tool to estimate the surface and core temperature dynamics. The two models are then coupled through the reversible plus irreversible heat generation and also via temperature dependence of the equivalent circuit model parameters. The modeled terminal voltage and surface temperature dynamics are in good agreement with experimental observations for fixed environmental temperature with forced air cooling.**

I. INTRODUCTION

Electric double layer capacitors (EDLC) are the premier electrochemical devices in terms of power density, long cycle life, and extreme temperature operation. Materials used for the electrode range from activated carbon to metal oxides and polymers. The electrolyte could be either aqueous or non-aqueous depending on the materials and application. The high power capability arises from the low equivalent series resistance (ESR) as a result of high electrolyte conductivity, low electronic resistance of the electrode and the interface between electrodes and current collectors. Formation of electric double layers at the interface of the electrode and electrolyte is due to electrostatic forces and as no chemical or phase changes occurs, the process is highly reversible and the charge-discharge cycle can be repeated virtually without limit [1]. Higher capacity in EDLC compared to dielectric capacitors is achieved by increasing the surface area using porous electrodes with an extremely large internal effective surface [2].

In real world application of ultracapacitors, it's vital to predict the electrical and thermal dynamics in a real time manner in order to meet the performance requirements of the load while maintaining the module in safe operating conditions. Efforts have been made on modeling the terminal voltage behavior of ultracapacitors in the frequency domain mainly using electrochemical impedance spectroscopy (EIS) [3]. Buller et al.'s equivalent electric circuit model has four parameters to be determined and considers dependence on four voltage levels and temperatures from -30°C to 50°C.

The proposed equivalent circuit model in this paper consists of a series resistance in series with a single R-C pair. This model has two states. The first state is the state of charge (SOC) of the ultracapacitor which is the amount of charge stored in the cell at each time over the maximum storable charge. The second state is the voltage across the R-C pair. The electric model has three parameters to be identified. Due to the wide range of operating conditions, temperature dependent model parameters are needed to accurately predict the system response. The parameters of the equivalent circuit model also depend on state of charge and current direction. In order to predict the module temperature we also need an accurate model of the heat transfer. The heat transfer problem can be reduced to a linear two state system similar to the model developed for cylindrical batteries in [4]. For ELDC however the reversible heat generation effect must also be considered. Experimental observation of the thermal dynamics and the relative contribution of reversible heat generation was shown in [5]. The thermal dynamics can be predicted by numerically solving the governing partial differential equations as investigated in [6]-[7]. However these complex first principle based thermodynamic models can not be solved in real time and therefore are not suitable for control applications. Utilizing a reduced order model with sufficient accuracy [5] is more preferable for the purposes of this study. The electrical and thermal models will be coupled to develop a computationally efficient electro-thermal model for cylindrical EDLC. This model can be used in precisely calculating the efficiency of ultracapacitors under different loads following the study conducted in [8]. Also the model could be utilized in system integration and control studies in the vehicle level.

II. ULTRACAPACITOR ELECTRICAL MODEL

In this section the electric model for the ultracapacitor is presented. An equivalent electric circuit model is proposed with the following characteristics:

- Fewer parameters to be identified compared with the detailed electrochemical model.

[1]Yasha Parvini and Ardalan Vahidi are with the Department of Mechanical Engineering, Clemson University, Clemson, SC 29634, USA sparvin@clemson.edu, avahidi@clemson.edu

[2]Jason B. Siegel and Anna G. Stefanopoulou are with the Department of Mechanical Engineering, University of Michigan, Ann Arbor, MI 48109, USA siegeljb@umich.edu, annastef@umich.edu

- Computational efficiency and suitability for control oriented studies.
- Accurate prediction of dynamic terminal voltage.

In this section the experimental setup for parametrization tests and also the identification results are presented.

A. Equivalent Electric Circuit Model

In this study the galvanostatic approach is used in the whole modeling procedure where current is the input to the system and the output is the terminal voltage. Fig. 1 shows the schematic of the equivalent electric circuit model. It consists of an equivalent series resistance which represents the internal resistance of the ultracapacitor and also R-C branches that capture the voltage behavior of the cell during relaxation. Positive current corresponds to charging and negative sign is for discharging. The dynamic model is derived by applying kirchhoff's voltage law (KVL) to the circuit shown in Fig. 1. The equation governing the terminal voltage could be written as follows:

$$V_T = OCV(SOC) + IRs + \sum_{j=1}^{n} V_{RC,j} \tag{1}$$

In (1), OCV is the open circuit voltage which is a linear function of state of charge for an ideal capacitor. The SOC is determined by coulomb counting by the following state equation:

$$\frac{dSOC}{dt} = \frac{I}{CV_{max}} \tag{2}$$

where C and V_{max} are the nominal capacitance of the ultracapacitor in Farads and the voltage across the ultracapacitor at maximum charge. The second part in (1), is the voltage drop over the ohmic resistance and the last part is the sum of voltage drops across parallel R-C circuits connected in series. The voltage dynamics of each R-C pair is described as:

$$\frac{dV_{RC,j}}{dt} = -\frac{1}{R_j C_j} V_{RC,j} + \frac{I}{C_j} \tag{3}$$

where R_j and C_j are the equivalent resistance and capacitance respectively. For example the state space representation of an ideal ultracapacitor knowing that $OCV = V_{max} * SOC$ and assuming a single R-C pair ($j = 1$) with V_1 voltage drop across it, is as follows:

$$\begin{bmatrix} \dot{SOC} \\ \dot{V_1} \end{bmatrix} = \begin{bmatrix} 0 & 0 \\ 0 & \frac{-1}{R_1 C_1} \end{bmatrix} \begin{bmatrix} SOC \\ V_1 \end{bmatrix} + \begin{bmatrix} \frac{1}{CV_{max}} \\ \frac{1}{C_1} \end{bmatrix} I \tag{4}$$

B. Experimental Setup

Experiments have been conducted on a Maxwell BCAP3000 cylindrical cell with activated carbon as electrodes. The nominal capacitance of the cell is 3000 Farads. The cell contains non-aqueous electrolyte allowing the maximum rated voltage of 2.7 Volts. All the experiments related to parametrization and validation of both the electrical and thermal models are conducted using the following set of equipments:

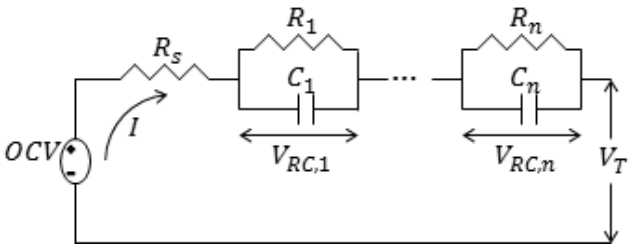

Fig. 1. Schematic of the equivalent electric circuit model with n number of RC branches

- Power supply: Bitrode FTV1-200/50/2-60 cycler which is capable of supplying up to 200A suitable for running the pulse-relaxation and also the driving cycle validation tests.
- Thermal chamber: Cincinnati sub-zero ZPHS16-3.5-SCT/AC capable of controlling the ambient temperatures as low as -40°C .

C. Electric Model Parameterization

The open circuit voltage V_{ocv}, capacitance C, series resistance R_s, resistance and capacitance of the R-C pairs are the parameters to be identified. V_{ocv} and C for charging are obtained by charging the ultracapacitor from zero to its maximum nominal voltage under a low current of 0.225A. The ultracapacitor is then discharged to zero with similar current rate to obtain the capacity and OCV for discharging. The difference between charging and discharging OCV is small due to low current and small internal resistance.

The parameters of the equivalent circuit including R_s, R_j, and C_j, are identified using pulse-relation experiments. Four current levels, 191, 135, 67.5 and 22.5 Amperes, are applied. In order to investigate the dependence of the parameters on SOC, sub-zero temperature, and also the direction of current, appropriate tests have been designed to sweep the whole SOC range (from 0 to 100 with 5% intervals) and temperatures ranging from -40°C to 0°C (-40, -20, 0°C) for both charging and discharging. Fig. 2 is one example of an SOC sweep at fixed temperature. In this specific test the temperature is -40°C and the ultracapacitor cell is charged with constant current of 191A from 0% SOC to 5% SOC. After a rest period of 20 seconds the same step is repeated in 5% SOC intervals till 100% SOC. Similarly the same procedure is repeated for discharging to also investigate the effect of current direction.

The identification is performed by minimizing the square error between the measured and simulated terminal voltages at each time instant at each fixed temperature level. The cost function is:

$$J = \sum_{k} (V_m(k) - V_T(k))^2 \tag{5}$$

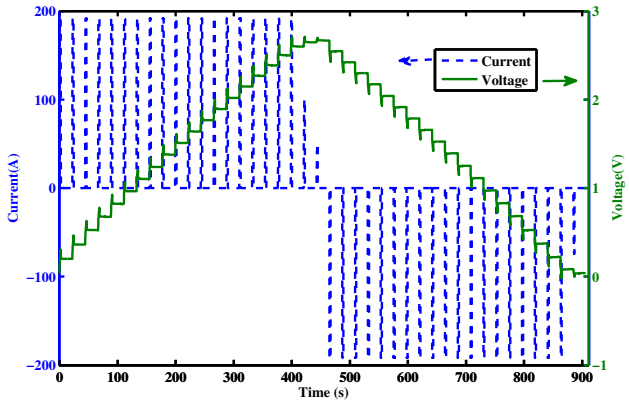

Fig. 2. Pulse-relaxation test at -40°C and 191A current

where $V_m(k)$ is the measured terminal voltage at each time and $V_T(k)$ is the simulated terminal voltage from equation (1). The number of R-C branches will be determined based on the fitting results in the next section.

D. Electric Model Identification Results

In this section the parameterization results are discussed. Firstly we start with a simple $OCV - R_s$ model and in the next steps the R-C branches are added, evaluating the performance of the model at each level. The parameters, (Rs, R-C) in the equivalent circuit model are temperature dependent, however through careful design of the experiments, by holding the temperature constant, they can be identified at a fixed temperature without considering the coupled thermal model.

The OCV of an ideal ultracapacitor as mentioned before is a linear function of SOC. In reality the OCV of the double layer ultracapacitor under investigation has a nonlinear relationship with SOC. Fig. 3 shows the OCV as a function of SOC in both the ideal and real cases at -40°C.

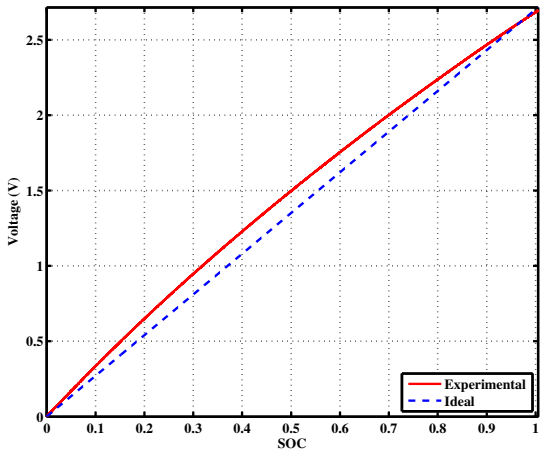

Fig. 3. Open circuit voltage vs state of charge for ideal and real cases at -40°C

This nonlinear OCV versus SOC profile is integrated into the model using a lookup table. The root mean square error (RMSE) numbers in Table I show that the real nonlinear OCV profile should be integrated in the model which decreases the RMSE error by 80%. The next step is to add an R-C branch to the $OCV - R_s$ model and evaluate the model accuracy. Fig. 4 compares the terminal voltage results from the $OCV - R_s - RC$ model and the experimental data for the experiment conducted at -20°C and 135A of current. The terminal voltage dynamics derived from the $OCV - R_s - RC$ model is in agreement with experimental data with a RMSE error of only 9 mV. This result shows that the $OCV - R_s - RC$ model is accurate enough and will be used as the final electrical model. Similarly the parameterization is performed for the other tests with different current rates and temperatures. Table II lists the values of the identified parameters for the tests with temperatures at -40,-20 and 0°C and 135A of current. Results show that the total impedance of the ultracapacitor increases as temperature decreases. This temperature dependence of identified electric parameters indicates the necessity of coupling the electric and thermal models.

TABLE I
RMSE BETWEEN MODEL AND EXPERIMENT

Model	RMSE (mV)
Linear-OCV-R_s	81
Nonlinear-OCV-R_s	16
OCV-R_s-RC	9

TABLE II
IDENTIFIED PARAMETERS FOR TEMPERATURES -40,-20 AND 0 °C AND 135A OF CURRENT

	−40°C	-20 °C	0 °C
$R_s(m\Omega)$	0.55	0.48	0.43
R_1 $(m\Omega)$	1	0.85	0.75
$C_1(F)$	45235	32940	32060

III. ULTRACAPACITOR THERMAL MODEL

The thermal model used in this study is adopted from a computationally efficient model originally developed for cylindrical batteries by Kim et al. [4]. First the two state thermal model is described. In the consecutive sections entropic heat generation and electro-thermal coupling are introduced. Finally parameterization results are presented.

A. Two State Thermal Model

The model is based on one dimensional heat transfer along the radial direction of a cylinder with convective heat transfer boundary conditions as illustrated in Fig. 5.

A cylindrical ultracapacitor, so-called a jelly-roll, is fabricated by rolling a stack of cathode/separator/anode layers. Assuming a symmetric cylinder, constant lumped thermal properties such as cell density, conduction heat transfer and specific heat coefficient are used [4]. Uniform heat generation

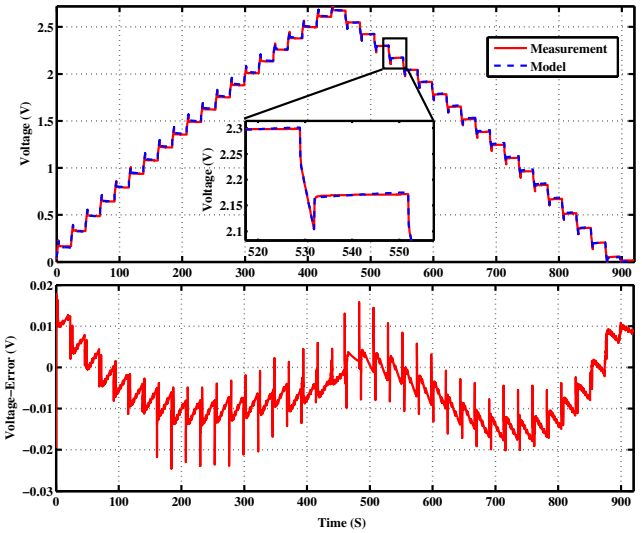

Fig. 4. Comparison between terminal voltage from experiments and the $OCV - R_s - RC$ model

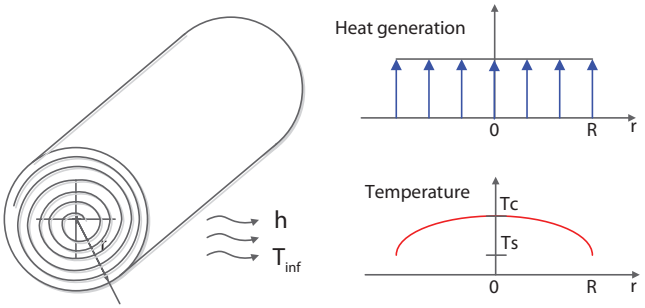

Fig. 5. Given the assumption of uniform heat generation with a convective cooling boundary condition at the surface, the radial temperature distribution can be modeled as a 4th order polynomial [4].

along the radial direction is a reasonable assumption according to [9]. The temperature distribution in the axial direction is more uniform than the radial due to higher thermal conductivity [10]. The radial 1-D temperature distribution is governed by the following PDE:

$$\rho c_p \frac{\partial T(r,t)}{\partial t} = k_t \frac{\partial^2 T(r,t)}{\partial r^2} + \frac{k_t}{r}\frac{\partial T(r,t)}{\partial r} + \frac{Q(t)}{V_{cell}} \tag{6}$$

with boundary conditions:

$$\frac{\partial T(r,t)}{\partial r} \mid_{r=0} = 0 \tag{7}$$

$$\frac{\partial T(r,t)}{\partial r} \mid_{r=R} = -\frac{h}{k_t}(T(R,t) - T_\infty) \tag{8}$$

where t, ρ, c_p and k_t are time, volume-averaged density, specific heat, and conduction heat transfer coefficients, respectively. The heat generation rate inside the cell is Q, The cell volume is V_{cell} and R is the radius of the cell. The first boundary condition in (7) is to satisfy the symmetric structure of the ultracapacitor around the core. Convective heat transfer at the surface of the cell forms the boundary condition in (8). Here T_∞ is the ambient air temperature and h is the heat transfer coefficient for convective cooling.

With uniform heat generation distribution the solution to (6) is assumed to satisfy the following polynomial temperature distribution as proposed in [11]:

$$T(r,t) = \alpha_1(t) + \alpha_2(t)(\frac{r}{R})^2 + \alpha_3(t)(\frac{r}{R})^4 \tag{9}$$

The volume-averaged temperature $\bar{T}$, and volume averaged temperature gradient $\bar{\gamma}$ are chosen as the states of the thermal model. These quantities can be related to the temperature distribution as follows:

$$\bar{T} = \frac{2}{R^2}\left[\int_0^R rT\,dr\right] \tag{10}$$

$$\bar{\gamma} = \frac{2}{R^2}\left[\int_0^R r(\frac{\partial T}{\partial r})\,dr\right] \tag{11}$$

Using (9) the surface T_s and core T_c temperature of the cell are expressed by:

$$T_s = \alpha_1(t) + \alpha_2(t) + \alpha_3(t), \qquad T_c = \alpha_1(t) \tag{12}$$

The temperature distribution $T(r,t)$ can be written as a function of $T_s, \bar{T}$ and $\bar{\gamma}$ after some algebraic manipulation. The original PDE (6), can be reduced to a set of two linear ODEs with the state space representation of:

$$\dot{x} = Ax + Bu, \quad y = Cx + Du \tag{13}$$

where $x = [\bar{T} \quad \bar{\gamma}]^T$, $u = [Q \quad T_\infty]^T$, and $y = [T_c \quad T_s]^T$ are state, input and output vectors respectively. The parameter $\beta = \frac{k_t}{\rho c_p}$ is the thermal diffusivity. Finally the linear system matrices A, B, C, and D are:

$$A = \begin{bmatrix} \frac{-48\beta h}{R(24k_t+Rh)} & \frac{-15\beta h}{24k_t+Rh} \\ \frac{-320\beta h}{R^2(24k_t+Rh)} & \frac{-120\beta(4k_t+Rh)}{R^2(24k_t+Rh)} \end{bmatrix}$$

$$B = \begin{bmatrix} \frac{\beta}{k_t V_{cell}} & \frac{48\beta h}{R(24k_t+Rh)}) \\ 0 & \frac{320\beta h}{R^2(24k_t+Rh)} \end{bmatrix}$$

$$C = \begin{bmatrix} \frac{24k_t-3Rh}{24k_t+Rh} & -\frac{120Rk_t+15R^2h}{8(24k_t+Rh)} \\ \frac{24k_t}{24k_t+Rh} & \frac{15Rk_t}{48k_t+2Rh} \end{bmatrix}$$

$$D = \begin{bmatrix} 0 & \frac{4Rh}{24k_t+Rh} \\ 0 & \frac{Rh}{24k_t+Rh} \end{bmatrix}$$

This linear two state model is easy to parameterize as shown in the following sections.

B. Irreversible and Reversible Heat Generation

The inclusion of reversible heat generation in the model is required to accurately predict the dynamic temperature response for cycling over different SOC ranges at both low and high currents. Fig. 6 shows a set of four experiments at -20°C and pulse current of 140A that highlights the effect of rest period between the charge and discharge cycle and depth of discharge on the dynamics of temperature rise. All profiles show an overall increase in the cell temperature during the test which is due to the irreversible heat generation rate due to resistive losses and is equal to:

$$Q_{joule} = R_s I^2 + V_{R_1C_1} I \tag{14}$$

where $V_{R_1C_1}$ is the voltage across the single R-C pair. The increase in temperature depends on the depth of discharge only when there is a rest period between the charge and discharge cycle. In this case the RMS current is lower and therefore Q_{joule} is smaller. While in the case without any rest between charging and discharging the average steady state temperature is not a function of SOC range. A closer look at the inset in Fig. 6 will also reveal that there is an obvious non-linearity in the temperature ripple. This is due to the reversible heat generation which is a result of entropy change during charge and discharge period. The temperature change is exothermic during charging and endothermic during discharging. The entropic heat generation rate is governed by [5]:

$$Q_{rev} = \delta \, \bar{T} \, I(t) \tag{15}$$

The reversible heat generation rate is proportional to current and the volume average temperature $\bar{T}$ with the unit of $(^\circ K)$. The constant of proportionality δ is related to the physical properties of the cell and will be estimated from the temperature measurements.

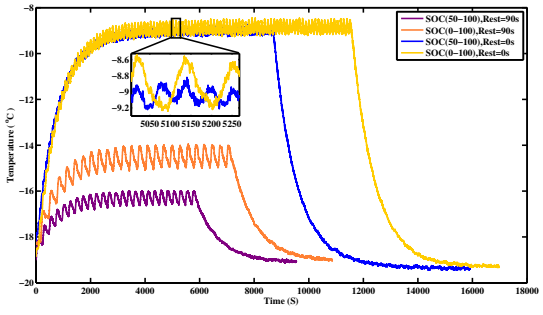

Fig. 6. Thermal pulse tests at -20°C and 140A for different SOC ranges and rests

C. Electro-Thermal Coupling

The electrical and thermal models are coupled to form the complete system model. The total heat generation rate is calculated from the equivalent circuit model, and the temperature (which is the output of the thermal model) feeds back into the resistance of the equivalent circuit. The resulting coupled model is non-linear. Figure 7 illustrates the coupled electro-thermal model.

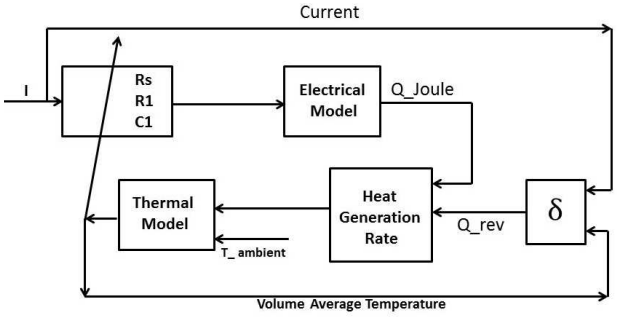

Fig. 7. Coupling of the electrical and thermal models

D. Thermal Test Procedure and Parameterization Results for the Thermal Model

Repeated cycling of the ultracapacitor is used to induce self heating. This temperature rise can be used for parameterization of the thermal model. The set of experiments in the thermal chamber are conducted at the temperature of -20°C. The thermocouple used for temperature measurements is T-type and is mounted on the surface of the cell. The core temperature is not measured in this study and therefore must be predicted by the model. Three current levels (140, 100, and 50 Amps) and two SOC ranges (0-100% and 50-100%) are used to generate a rich data set. In each set of experiments a discharged or a half charged cell undergoes cycles of charge-rest-discharge until the surface temperature of the cell reaches steady state followed by a long rest period till the surface temperature relaxes to its initial value. Fig. 8 shows the temperature and voltage evolution under a pulse test with current of 140A. In this test the cell is cycled in the upper half of the voltage range (50-100% SOC) with an ambient temperature of -20°C and 90 seconds of rest between every charge and discharge period. The temperature reaches steady state after approximately 1 hr. The temperature relaxation data is also useful for parameterizing the heat capacity and coefficient of convective cooling in the model.

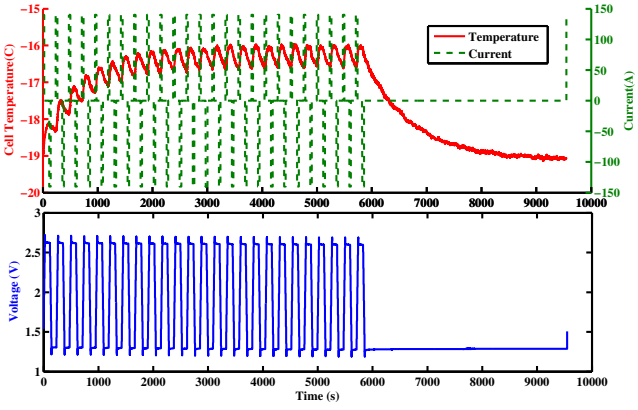

Fig. 8. Test procedure for thermal model parameterization

The convective h and conductive k_t heat coefficients, specific heat coefficient C_p and a parameter associated with reversible heat generation δ are identified for the thermal model. The physical parameters of the cell that are measurable are summarized in Table III.

TABLE III
PHYSICAL PARAMETERS OF THE ULTRACAPACITOR CELL

Mass (Kg)	length	Radius	Volume	Density
0.51Kg	0.138m	0.0304m	4E-4m^3	1277 $\frac{Kg}{m^3}$

The parameterization is performed by minimizing the square error between the measured and simulated surface temperatures. The cost function to be minimized is:

$$J = \sum_k (T_m(k) - T_s(k))^2 \tag{16}$$

Fig. 9 shows the parameterization results for the test conducted at -20°C ambient air temperature and pulse current of 140A with zero rest and SOC ranging from 0 to 100. The total heat generation rate is calculated through the electrical model and fed into the thermal model. The electrical model parameters are fixed and are derived from the -20°C and 135A pulse-relaxation test. The RMS error is only 0.13°C which is an indicator of the thermal model accuracy. Table IV shows the results for the identified thermal parameters.

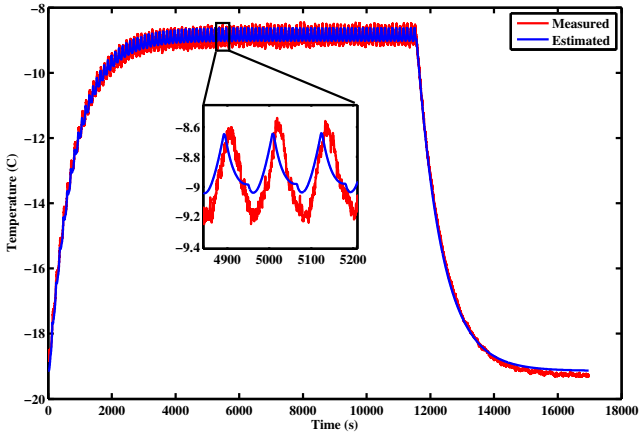

Fig. 9. Parameterization result for -20°C ,140A, zero rest and SOC range of 0 to 100

The value estimated for h is in the range of forced convective heat transfer coefficient for air which is between 10 to 200 $W/(m^2K)$. The specific heat coefficient is 2256 $W/(m^2K)$ which is expected to be close to the amount of the cell's organic based electrolyte (Acetonitrile c_p=2259 J/kgK at -20 °C). The thermal conductivity of 2.42W/mK at -20 °C is a result of the combined thermal conductivity of activated carbon, electrolyte, separator and the aluminum current collectors formed in a jelly roll shape. The value of 0.00022 for δ at -20 °C is comparable to 0.00033 J coulomb^{-1} K^{-1} reported in [5] for a 2.7 V, 5000 F prismatic cell with organic electrolyte at room temperature.

TABLE IV
IDENTIFIED THERMAL PARAMETERS FOR THE TEST AT -20°C ,140A, ZERO REST AND SOC RANGE OF 0 TO 100

Parameter	*Value*	*Unit*
h	68.8	W/m2.K
c_p	2256	J/kgK
k_t	2.42	W/mK
δ	0.00022	J/coulomb.K

IV. CONCLUSIONS

This paper shows the parameterization of a four state electro-thermal model for cylindrical double layer ultracapacitors including entropic (reversible) heat generation that is accurate for sub-zero temperatures. In the future this computationally efficient model can be used for real time vehicle level control such power management, battery life extension through hybridization, cold starting of engines and also efficiency analysis of ultracapacitors.

ACKNOWLEDGMENT

The authors wish to acknowledge the technical and financial support of automotive research center (ARC) in accordance to agreement W56HZV-04-2-0001 with TARDEC.

REFERENCES

[1] J. B. Goodenough, H. Abruna, and M. Buchanan, "Basic research needs for electrical energy storage," in *Report of the basic energy sciences workshop for electrical energy storage*, vol. 186, 2007.
[2] R. Kötz and M. Carlen, "Principles and applications of electrochemical capacitors," *Electrochim. Acta*, vol. 45, no. 15, pp. 2483–2498, 2000.
[3] S. Buller, E. Karden, D. Kok, and R. W. De Doncker, "Modeling the dynamic behavior of supercapacitors using impedance spectroscopy," *IEEE Transactions on Industry Applications*, vol. 38, 2002.
[4] Y. Kim, S. Mohan, J. Siegel, A. Stefanopoulou, and Y. Ding, "The estimation of temperature distribution in cylindrical battery cells under unknown cooling conditions," *Control Systems Technology, IEEE Transactions on*, vol. PP, no. 99, pp. 1–1, 2014.
[5] J. Schiffer, D. Linzen, and D. U. Sauer, "Heat generation in double layer capacitors," *J. Power Sources*, vol. 160, no. 1, pp. 765–772, 2006.
[6] H. Gualous, H. Louahlia, and R. Gallay, "Supercapacitor characterization and thermal modelling with reversible and irreversible heat effect," *Power Electronics, IEEE Transactions on*, vol. 26, no. 11, pp. 3402–3409, 2011.
[7] A. d'Entremont and L. Pilon, "First-principles thermal modeling of electric double layer capacitors under constant-current cycling," *J. Power Sources*, vol. 246, pp. 887–898, 2014.
[8] Y. Parvini and A. Vahidi, "Optimal charging of ultracapacitors during regenerative braking," in *Electric Vehicle Conference (IEVC), 2012 IEEE International*. IEEE, 2012, pp. 1–6.
[9] D. H. Jeon and S. M. Baek, "Thermal modeling of cylindrical lithium ion battery during discharge cycle," *Energy Conversion and Management*, vol. 52, no. 8, pp. 2973–2981, 2011.
[10] H. Maleki, S. Al Hallaj, J. R. Selman, R. B. Dinwiddie, and H. Wang, "Thermal properties of lithium-ion battery and components," *J. Electrochem. Soc.*, vol. 146, no. 3, pp. 947–954, 1999.
[11] V. R. Subramanian, V. D. Diwakar, and D. Tapriyal, "Efficient macro-micro scale coupled modeling of batteries," *J. Electrochem. Soc.*, vol. 152, no. 10, pp. A2002–A2008, 2005.